Case Studies in Thermal Engineering 44 (2023) 102827

Contents lists available at ScienceDirect

Case Studies in Thermal Engineering

journal homepage: www.elsevier.com/locate/csite

Natural convection of large Prandtl number fluids: A controversy answered by a new thermal lattice Boltzmann model

Sheng Chen [a,*], Kai H. Luo [b], Amit Kumar Jain [a], Dharminder Singh [a], Don McGlinchey [a]

[a] School of Computing, Engineering and Built Environment, Glasgow Caledonian University, Glasgow G4 0BA, UK
[b] Department of Mechanical Engineering, University College London, London WC1E 7JE, UK

ARTICLE INFO

Keywords:
Natural convection
Lattice Boltzmann
Prandtl number
Nusselt number
Multiple-relaxation-time (MRT) model

ABSTRACT

The purpose of this work is to deepen our understanding of natural convection with large Prandtl number fluids and to resolve some controversies in the previous publications. To achieve this purpose, a new thermal multiple-relaxation-time lattice Boltzmann model is proposed. Natural convection in a square cavity, a benchmark test case, is investigated numerically using the new model. The Prandtl number is up to 100. For the first time, it is numerically observed that there are two critical Prandtl numbers in the natural convection, which will affect the correlation between the Nusselt number and Prandtl number critically. Three heat transfer characteristic ranges of natural convection are defined in this work, according to the two critical Prandtl numbers. In each range, the dominant heat transfer mechanism is different, which can solve a long-standing issue in the discipline of heat and mass transfer: completely opposing statements on the correlation between the Nusselt number and Prandtl number for natural convection, were published in the open literature. For the first time, this work reveals cause behind the controversial reports and provides the guidance for the future research.

1. Introduction

Natural convection is an important process for energy transport in both the nature and industries, such as the cooling techniques adopted in chemical plants [1–4]. A deeper understanding of natural convection is very essential in the discipline of heat and mass transfer. Natural convection is still a "hot" scientific topic in the domain of fundamental research. Although it has been investigated intensively and it has been involved in many research publications.

Most of the available relevant literature only focuses on natural convection of low Prandtl number (i.e. $Pr < 1$) working fluids, such as air [5–7]. The latest progress in this area has been achieved by the review paper [8]. On the contrary, the open research on the influence of large Pr on natural convection is relatively limited, although high Pr fluids are commonly found in industrial and engineering applications, such as molten organic phase change materials for thermal energy storage [9] or thermal management [10], organic liquid coolants for cooling of fuel cells [11], and black liquor in kraft pulp production processes [12]. More unfortunately, some of them even raised opposing statements. Das and Bhattacharya [13] numerically investigated the effect of Pr on natural convection and Pr is up to 10. They suggested that heat transfer would be depressed by a large Pr, which is completely opposed to the conclusion listed in Ref. [14]. In the work by Hsieh and Wang [14], natural convection in a cavity was studied experimentally, with $Pr = 0.7, 6$ and 464. Based on their experimental data, the authors summarized that heat transfer

* Corresponding author.
E-mail address: sheng.chen@gcu.ac.uk (S. Chen).

https://doi.org/10.1016/j.csite.2023.102827
Received 9 November 2022; Received in revised form 13 February 2023; Accepted 15 February 2023
Available online 18 February 2023

in natural convection would be weakly enhanced by a large Pr. Shishkina and his collaborators [15] numerically investigated the scaling relations in large Pr natural convection. They found heat transfer rates in natural convection would increase with Pr. Dubrulle [16] also concentrated on the scaling relations in large Pr natural convection. However, the author claimed heat transfer intensity would slightly decreased against Pr. Al-Amir et al. [17] simulated natural convection in a cavity filled by porous media and discussed the effect of Pr on heat transfer. Their numerical results illustrated that the average Nusselt (Nu) number did not depend on Pr monotonously. Natural convection in a square cavity driven by non-uniformly heating was studied numerically in the work by Basak et al. [18]. The authors proposed a correlation between Nu and Pr for $Pr = 0.7, 10$ and they stated heat transfer rates in natural convection would ascend with Pr. Thus far, to the best knowledge of the present authors, there is still no open literature which conducts a comprehensive study on the role of large Pr in natural convection, to resolve the above conflicted reports. In addition, thermal energy storage systems are becoming more and more important for modern renewable energy industries. For thermal energy storage systems, large Pr materials (usually $Pr \geq 10$, such as organic phase change materials) are adopted as working media. Consequently, the dependence of flow pattern and heat transfer features of natural convection on large Pr, should be revealed more clearly. Such effort is crucial for the research and development of the future high efficient thermal energy storage systems.

During the past decades, the lattice Boltzmann method (LBM) has matured as a powerful numerical tool for natural convection simulation as the LBM has several advantages, such as easy parallel computation and efficient complicated boundary treatment [19, 20]. To model natural convection of MHD (magnetohydrodynamic) nanofluid in a cavity, Sajjadi et al. [21] proposed a double MRT (multiple-relaxation-time) LBM approach. The effect of the Hartmann number on natural convection was numerically investigated in Ref. [21]. Natural convection in horizontal concentric annulus was simulated in Ref. [22]. The authors designed a LBM flux solver to reveal the influence of the total variation in fluid properties on flow patterns and heat transfer rates in the annulus. In order to address the challenge of natural convection with large temperature differences, Feng and his cooperators [23] established a new thermal LBM model. They showed that their model can work well for high Rayleigh (Ra) number natural convection and can capture oscillations of heat and mass transfer in large temperature gradient conditions. A high-order compact finite-difference LBM model was developed in Ref. [24] for a finer near-wall grid resolution without high computational cost, comparing with the traditional LBM. The authors employed their model to discuss the effects of Ra on natural convection constricted by complicated geometries. Sharma et al. [25] applied the cascaded thermal LB model for high Ra natural convection in a square cavity and concluded that the cascaded thermal LB model has good numerical stability for turbulent natural convection simulation . Then the cascaded thermal LB model was extended to natural convection in a cavity filled by porous media [26]. Dapelo et al. [27] developed a LBM model for advection–diffusion flows with a wide range of Péclet numbers and they analyzed the numerical stability accordingly. Here only a few can be cited due to the huge amount of the literature. However, so far there are no LBM models, especially no MRT LBM models, for natural convection with large Pr working fluids, as a large Pr will cause a serious discrepancy between the relaxation time for velocity field and that for temperature field in the LBM, which can result in numerical instability.

To address the challenge and deepen our understanding on large Pr natural convection, in this work the influence of large Pr is revealed for the first time by analyzing the heat transfer patterns of natural convection in a square cavity numerically. A new MRT thermal LBM model, which extends the applicability of the LBM to natural convection with large Pr fluids, is proposed as the numerical tool for the investigation. The investigated domain is presented in Section 2. Then the governing equations are listed in Section 3 and the validation is given in Section 4. The discussion is presented in Section 5 and finally in Section 6 the conclusion is made. The novelty of this work is twofold: (1) a novel LBM model is proposed for high Pr fluid simulation and (2) a controversy in available literature for high Pr buoyant flow is solved.

2. Investigated domain and boundary conditions

Natural convection in a square cavity, as illustrated in Fig. 1, is investigated in this work. It is a benchmark test case for natural convection research [23–25,28]. The dimensionless temperature $T_h = 0.5$ and $T_l = -0.5$. The dimensionless width of the square cavity reads $H = 1.0$. In the present research, the cavity is filled with working fluids whose Prandtl number varies over $1 \leq Pr \leq 100$.

The dimensionless governing equations for the benchmark read [25,28]:

$$\nabla \cdot \vec{u} = 0 \tag{1}$$

$$\frac{\partial \vec{u}}{\partial t} + \vec{u} \cdot \nabla \vec{u} = -\nabla p + \nu \Delta \vec{u} - PrT \frac{\vec{g}}{|\vec{g}|} \tag{2}$$

$$\frac{\partial T}{\partial t} + \vec{u} \cdot \nabla T = \alpha \Delta T \tag{3}$$

where $\nu = PrRa^{-0.5}$ and $\alpha = Ra^{-0.5}$ are the normalized viscosity and thermal diffusivity, respectively, and Ra is the Rayleigh number. And p and T are the normalized pressure and temperature, respectively. In addition, $\vec{u} = (u_x, u_y)$ is the normalized velocity vector. The gravity $\vec{g}$ is downward. The detailed normalization process can be found in [29]

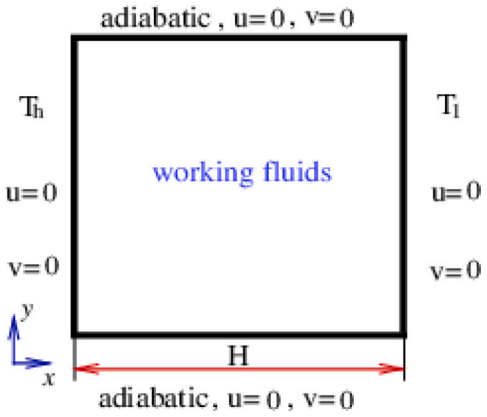

Fig. 1. Schematic configuration of the investigated domain.

3. Lattice Boltzmann model

3.1. Lattice Boltzmann model for flow field

The MRT LB model for the flow field (namely the governing equations Eqs. (1)–(2)), employed in our previous work [28], is adopted in this study, which read:

$$g_k(\vec{x}+\vec{e}_k\Delta t, t+\Delta t) - g_k(\vec{x},t) = \Omega_k(g) + \Delta t F_k \tag{4}$$

where $g_k(\vec{x},t)$ is the pseudo-particle distribution function with the discrete velocity $\vec{e}_k$. Δt and Δx are the dimensionless time interval and lattice grid spacing. Moreover, F_k is the discrete forcing, and $\Omega_k(g)$ is the discrete collision term. For a MRT model, $\Omega_k(g)$ reads:

$$\Omega_k(g) = -\sum_j (\mathbf{N}^{-1}\mathbf{S_f}\mathbf{N})_{jk}(g_j - g_j^{(eq)}) \tag{5}$$

where $g_j^{(eq)}$ is the discrete equilibrium distribution function. For the D2Q9 model, the relaxation matrix $\mathbf{S_f} = diag(1, 0.2, 0.1, 1, 1.2, 1, 1.2, 1/\tau, 1/\tau)$ and the transform matrix $\mathbf{N}$ can be found in [28]. Furthermore, there is

$$g_k^{(eq)} = \omega_k \rho[1 + \frac{c\vec{e}_k\cdot\vec{v}}{c_s^2} + \frac{(c\vec{e}_k\cdot\vec{v})^2}{2c_s^4} - \frac{|\vec{v}|^2}{2c_s^2}] \tag{6}$$

where the weight $\omega_0 = 4/9$, $\omega_{1\sim4} = 1/9$ and $\omega_{5\sim8} = 1/36$. c_s is the speed of sound. The discrete forcing term F_k can be evaluated by

$$F_k = \mathbf{N}^{-1}(\mathbf{I} - \frac{1}{2}\mathbf{S_f})\mathbf{N}_{jk}\overline{F}_k \tag{7}$$

where

$$\overline{F}_k = \omega_k[\frac{\vec{e}_k\cdot\vec{F}}{c_s^2} + \frac{(\vec{e}_k\cdot\vec{v})(\vec{e}_k\cdot\vec{F})}{c_s^4} - \frac{\vec{v}\cdot\vec{F}}{c_s^2}] \tag{8}$$

and $\mathbf{I}$ is the unity matrix. The velocity $\vec{v}$ is obtained by

$$\vec{v} = \sum_{k\geq 0}\vec{e}_k g_k + \frac{\Delta t}{2}\vec{F} \tag{9}$$

where

$$\vec{F} \equiv PrT\frac{\vec{g}}{|\vec{g}|} \tag{10}$$

The viscosity is obtained by

$$\nu = (\tau - 0.5)c_s^2\Delta t \tag{11}$$

3.2. Lattice Boltzmann model for temperature field

In order to simulate high Pr thermal fluids, in this work a new LBM MRT model is constructed for temperature field. The LBM evolution equation for the temperature field reads [28,30]

$$f_j(\vec{x}+\vec{e}_j\Delta t, t+\Delta t) - f_j(\vec{x},t) = \Omega_k(f_j) \tag{12}$$

For the MRT model, there is

$$\Omega_k(f_j) = -\sum_j (\mathbf{M}^{-1}\mathbf{S})_{jk}(m_j - m_j^{(eq)}) \tag{13}$$

where $\mathbf{M}$ is the transformation matrix and $\mathbf{S}$ is the relaxation matrix. In addition, $m_j = \mathbf{M}f_j$ is the moment of distribution function f_j in the phase space and $m_j^{(eq)}$ is the corresponding equilibrium moment [31]. For the D2Q5 lattice model, there are [31]

$$\mathbf{M} = \begin{pmatrix} 1 & 1 & 1 & 1 & 1 \\ 0 & 1 & -1 & -1 & 1 \\ 0 & 1 & 1 & -1 & -1 \\ -4 & 1 & 1 & 1 & 1 \\ 0 & 1 & -1 & 1 & -1 \end{pmatrix} \tag{14}$$

and $\mathbf{S} = diag(1, \tau_\Theta^{-1}, \tau_\Theta^{-1}, s_3, s_4)$, where $0 < s_3, s_4 < 2$ are the adjustable parameters [31]. For our new MRT model, $m_j^{(eq)}$ is proposed as

$$m_0^{(eq)} = \frac{T}{\eta}, m_1^{(eq)} = \frac{u_x T}{\eta}, m_2^{(eq)} = \frac{u_y T}{\eta}, m_3^{(eq)} = 2(1 - \frac{2}{\eta})T, m_4^{(eq)} = 0 \tag{15}$$

The temperature T is evaluated by

$$T = \eta \sum_j f_j \tag{16}$$

and the thermal diffusivity α is calculated by

$$\alpha = c_s^2 \eta(\tau_\Theta - 0.5)\Delta t \tag{17}$$

For the D2Q5 lattice model there exists $c_s^2 = 1/5$.

Through the multiscale expansion [30,31], the macroscopic governing equation for the temperature field, namely Eq. (3) can be recovered from Eq. (12). The detail please refer to Appendix.

In the existing LBM models for natural convection simulation, the correlation between α and τ_Θ is given by [28,31]

$$\alpha = c_s^2(\tau_\Theta - 0.5)\Delta t \tag{18}$$

For high Pr natural convection, $\alpha = \nu/Pr$ will be very small, which indicates τ_Θ will be extremely close to 0.5. However, if τ_Θ approaches to 0.5, the LBM will suffer from numerical instability [32]. To address such numerical instability, usually a very fine grid resolution has to be employed for the existing LBM thermal models, which implies high computational cost. In the present new LBM model, the extra parameter η in Eq. (17) provides a measure to sort out such challenge, without cost of finer grid resolutions. In the present simulation, the option for η reads:

$$\eta = 1/Pr, \qquad (Pr \geq 1) \tag{19}$$

In the present work, the non-equilibrium extrapolation boundary treatment employed in our previous simulation [32] is adopted to treat the boundaries.

4. Numerical validation

Two benchmark test cases of high Pr natural convection are employed for numerical validation.

Firstly, natural convection in a square cavity driven by non-uniformly heating, investigated in [18], is adopted to validate the present numerical approach. For such natural convection, $Pr = 10$. A grid resolution 128×128 is adopted.

The isotherms and stream lines are plotted in Fig. 2, for $Pr = 10$ and $Ra = 10^5$. Some thermal boundary layers can be observed near the solid walls, as illustrated by the temperature gradients therein. Thanks to the hot bottom, there emerge two symmetric vortices in the cavity: one is clockwise but the other is anti-clockwise. The circulations are strong in the vicinity of the center of the enclosure but become weak near the walls. Due to the strong circulations at the top half of the cavity, there the temperature differences are small and a big stratification area of temperature forms in the vicinity of the vertical symmetry line owing to stagnation of the buoyant flow. The isotherms and stream lines all are symmetric respect to the vertical central line of the investigated domain. The flow field and temperature field obtained by the present LBM approach agree well with those reported in [18].

The profiles of local Nusselt number at the bottom wall and the side wall are shown in Fig. 3. For comparison, the data published in [18] are also depicted. Owing to stagnation of the buoyant flow, convective heat transfer is weakened in the vicinity of the center of the bottom wall. In addition, the heat transfer rate on the top half of the side wall is bigger than its low half counterpart, due to the strong circulations which exist at the top half of the cavity. The present prediction is well quantitatively consistent to those reported in [18].

Grid-independence check is also conducted, as shown by Fig. 4. Two different grid densities 128×128 and 512×512 are employed. The grid density 128×128 can produce grid-independent simulation results for the high Pr natural convection investigated in this work.

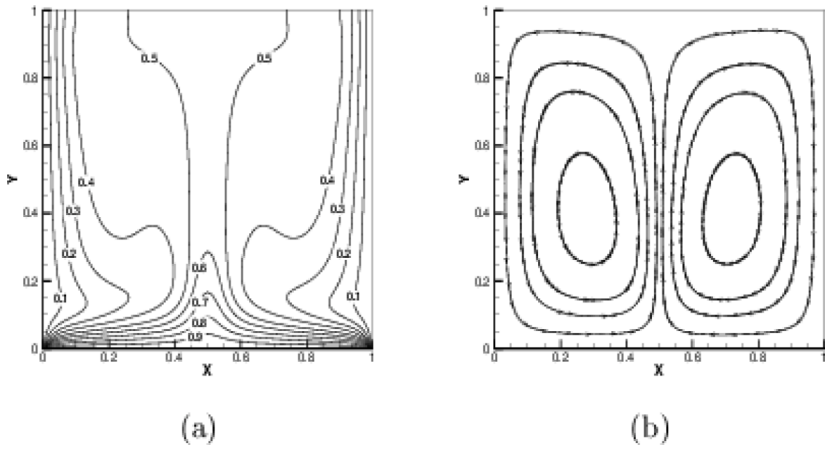

Fig. 2. (a) Isotherms, and (b) stream lines for natural convection in a square cavity driven by non-uniformly heating.

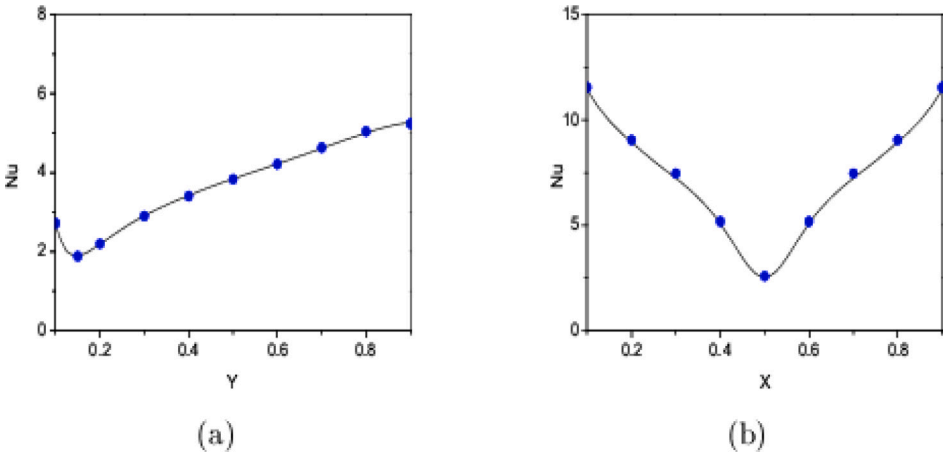

Fig. 3. Profiles of local Nusselt number (a) side wall, and (b) bottom wall for $Pr = 10$ and $Ra = 10^5$: line-present results, dot-data in [18].

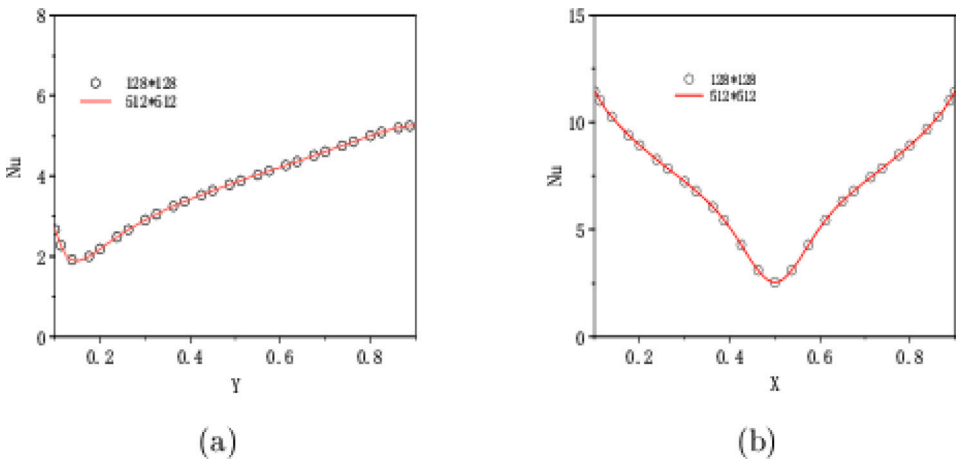

Fig. 4. Profiles of local Nusselt number (a) side wall, and (b) bottom wall for $Pr = 10$ and $Ra = 10^5$: line-grid density 512 × 512, circle-grid density 128 × 128.

Secondly, the Rayleigh–Bénard convection of high Prandtl number fluid ($Pr = 100$) [15] is simulated, with the grid resolution 128 × 128. Table 1 listed the average Nusselt number on the heating wall, versus different Rayleigh numbers. The present numerical

Table 1
Average Nusselt number on the heating wall with $Pr = 100$.

	Nu		
	[15]	Present	Error
$Ra = 10^4$	1.94	1.9655	1.3%
$Ra = 10^5$	3.83	3.7676	1.6%
$Ra = 10^6$	7.97	7.9351	0.4%

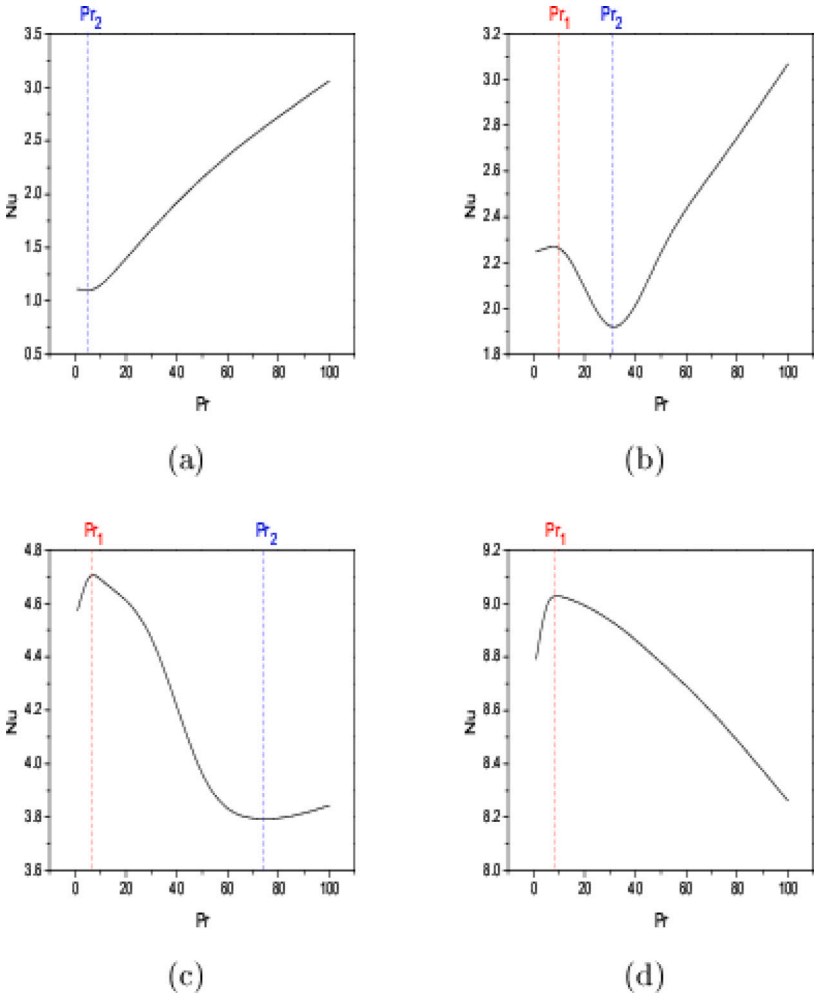

Fig. 5. Variation of Nu on the hot wall against Pr when (a) $Ra = 10^3$, (b) $Ra = 10^4$, (c) $Ra = 10^5$ and (d) $Ra = 10^6$.

results are in good agreement with the published data [15], which further demonstrates the capability of the present LBM approach for high Pr thermal buoyant flows. If the standard MRT model [28] was used, numerical instability would appear for the case $Ra = 10^6$ with $Pr = 100$.

5. Numerical simulation and discussions

Fig. 5 illustrates the variation of Nu against Pr at different Ra. One can observe that Nu depends on Pr complicatedly for most situations and Ra plays a key role affecting the relationship between Pr and Nu. For $Ra = 10^3$, the heat transfer is augmented monotonically with the increasing of Pr except $Pr < 5$ (for $1 < Pr < 5$, Nu goes down very slightly against the increment of Pr). When $Ra = 10^4$ or 10^5, firstly Nu ascends with Pr to reach a peak and then decreases quickly down to a minimum value, followed by another climbing. As $Ra = 10^6$, the heat transfer rate is enhanced with the increment of Pr but soon depressed by a higher Pr. Since $Ra > 10^4$, one can observe that Nu does not depend on Pr monotonically.

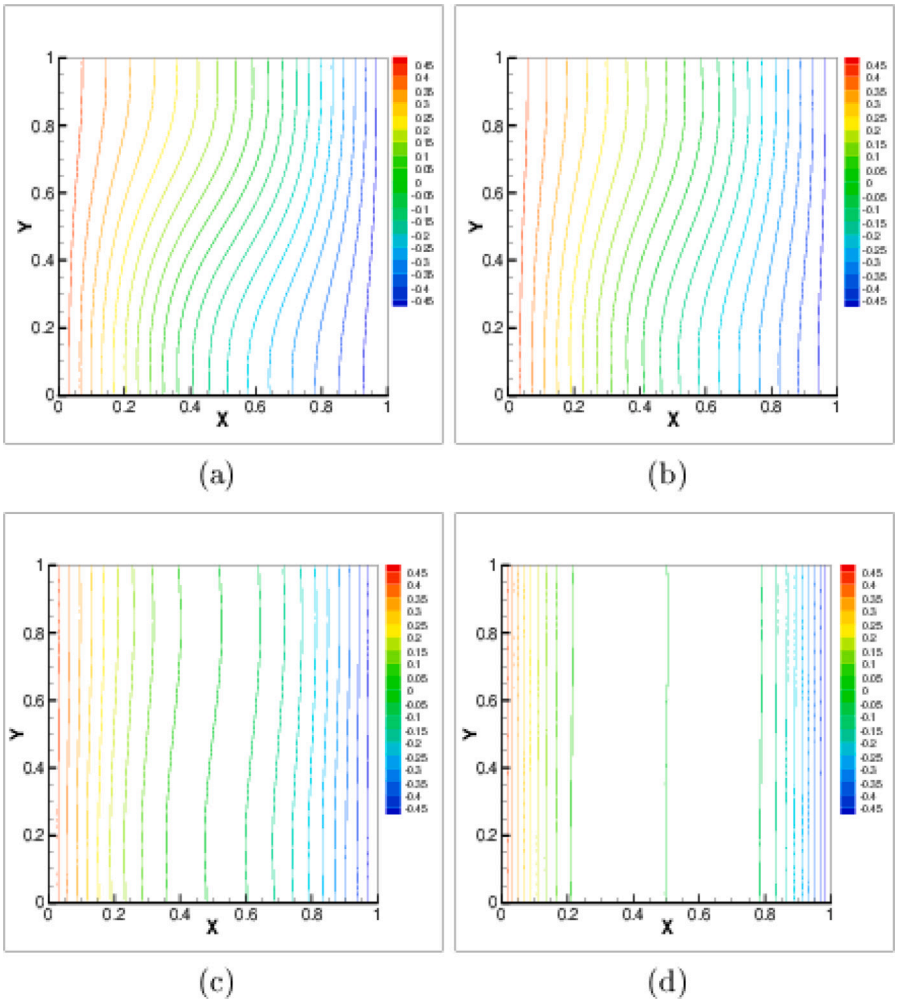

Fig. 6. Isotherms at (a) $Pr = 1$, (b) $Pr = 10$, (c) $Pr = 30$ and (d) $Pr = 100$ when $Ra = 10^3$.

Is there any simple rule hidden behind such complicated variation? To the best knowledge of the present authors, thus far there is nobody answering this question. In this work, it is tried to be revealed by analyzing the dominant heat transfer mechanism in the natural convection, with different Pr.

When Ra is small, for example $Ra = 10^3$, the dominant heat transfer mechanism in natural convection is heat conduction and the contribution due to heat convection can be omitted, as depicted by Fig. 6. The isotherms in Fig. 6 all are stratified and nearly vertical, for any value of Pr. For a higher Pr that implies a thinner thermal boundary layer [5–7], the density of isotherms in the neighbor of the vertical walls increases obviously. Such large temperature gradients cause more intensive heat transfer on the vertical walls. On the contrary, the isotherms in the center of the cavity become sparse, which indicates the temperature distributions are relatively smooth near the center. When $Pr \leq 10$, the plots of the isotherms near the vertical walls change slightly against Pr, so Nu does not vary obviously. With the aid of Fig. 6, it can be concluded that if heat conduction always plays a predominant role in natural convection, Nu will be augmented by working fluids with a higher Pr.

However, for natural convection with $Ra = 10^4$, there is a "hot" competition between heat conduction and heat convection when Pr varies. While $Pr \leq 10$, heat convection becomes the strongest driving force, as illustrated by Fig. 7(a)–(b): the isotherms in the vicinity of the center of the enclosure are nearly horizontal. Although the increasing of Pr will depress heat convection as a larger Pr will cause a thinner thermal boundary layer [5–7], if heat convection can keep its dominant role, Nu can ascend with Pr due to the increasing temperature gradients in the thinner thermal boundary layers. However, since $Pr > 10$, the contribution due to heat conduction becomes comparable to that due to heat convection, as shown by Fig. 7(c), where the isotherms in the center of the cavity come to be vertical. The transition of the predominant contributor causes the decrease of Nu against the growth of Pr. As $Pr > 30$, heat conduction plays a critical role and the contribution due to heat convection can be ignored, illustrated by Fig. 7(d)–(e), in which almost all isotherms are vertical. And in the heat-conduction-dominated range, Nu is enhanced by Pr, which agrees with the conclusion drawn above from the cases with $Ra = 10^3$. Through the analysis on the cases with $Ra = 10^4$, one can summarize

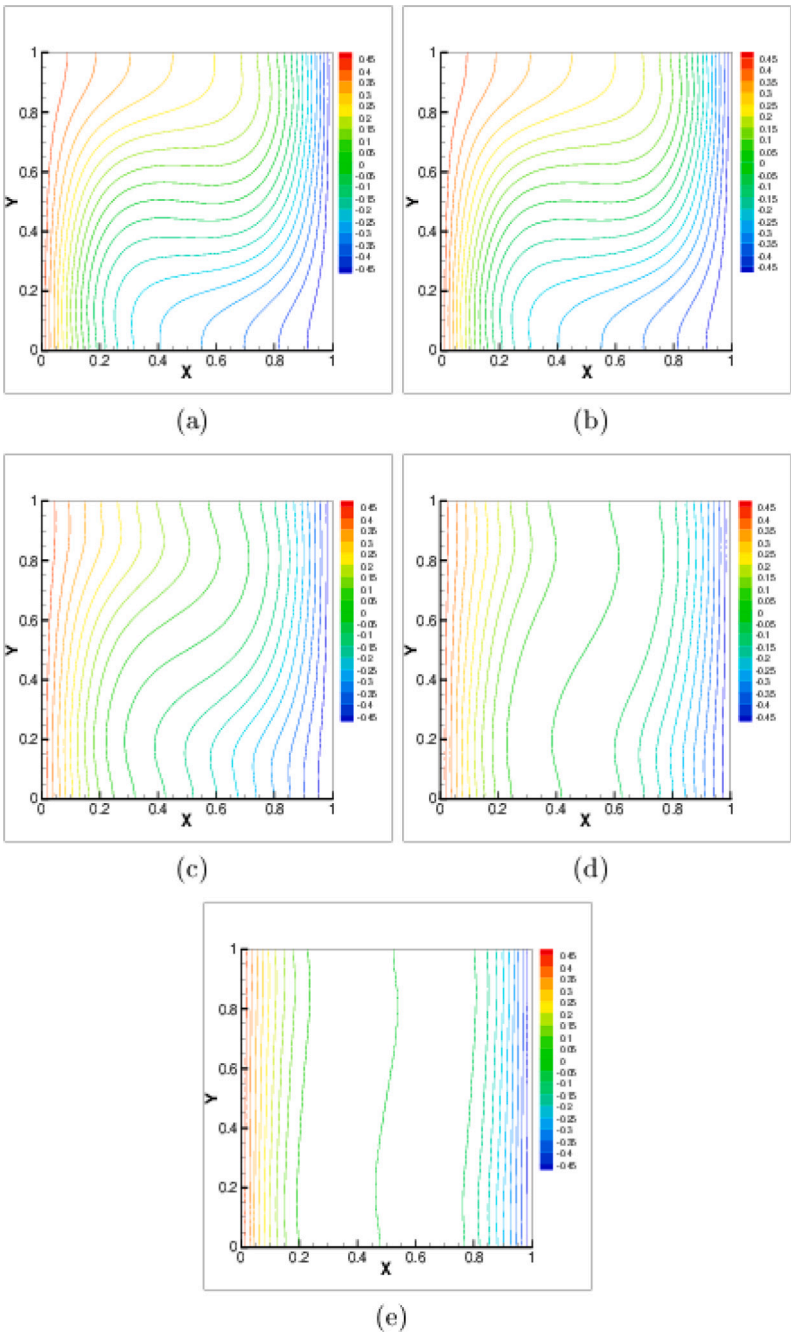

Fig. 7. Isotherms at (a) $Pr = 1$, (b) $Pr = 10$, (c) $Pr = 30$, (d) $Pr = 50$, and (e) $Pr = 100$ when $Ra = 10^4$.

that either in the heat-conduction-dominated natural convection or in the heat-convection-dominated natural convection, Nu will increase with Pr. But in the transition range where the predominant heat transfer mechanism becomes changing (e.g. from heat convection to heat conduction), Nu will be reduced against Pr.

The above conclusion can be proven again by the cases with $Ra = 10^5$. While $Pr \leq 10$, heat convection is the major contributor to heat transfer and the contribution of heat conduction can be omitted, as shown by Fig. 8(a)–(b), in which most of the isotherms in the cavity are horizontal. Within this range, heat transfer due to the motion of working fluids will be intensified by the increment of Pr. For $10 < Pr < 70$, as illustrated by Fig. 8(c)–(d), the horizontal isotherms become vanishing and are replaced by the vertical isotherms, which implies heat conduction is overweighing heat convection. No doubt, Within this transition zone $10 < Pr < 70$, Nu

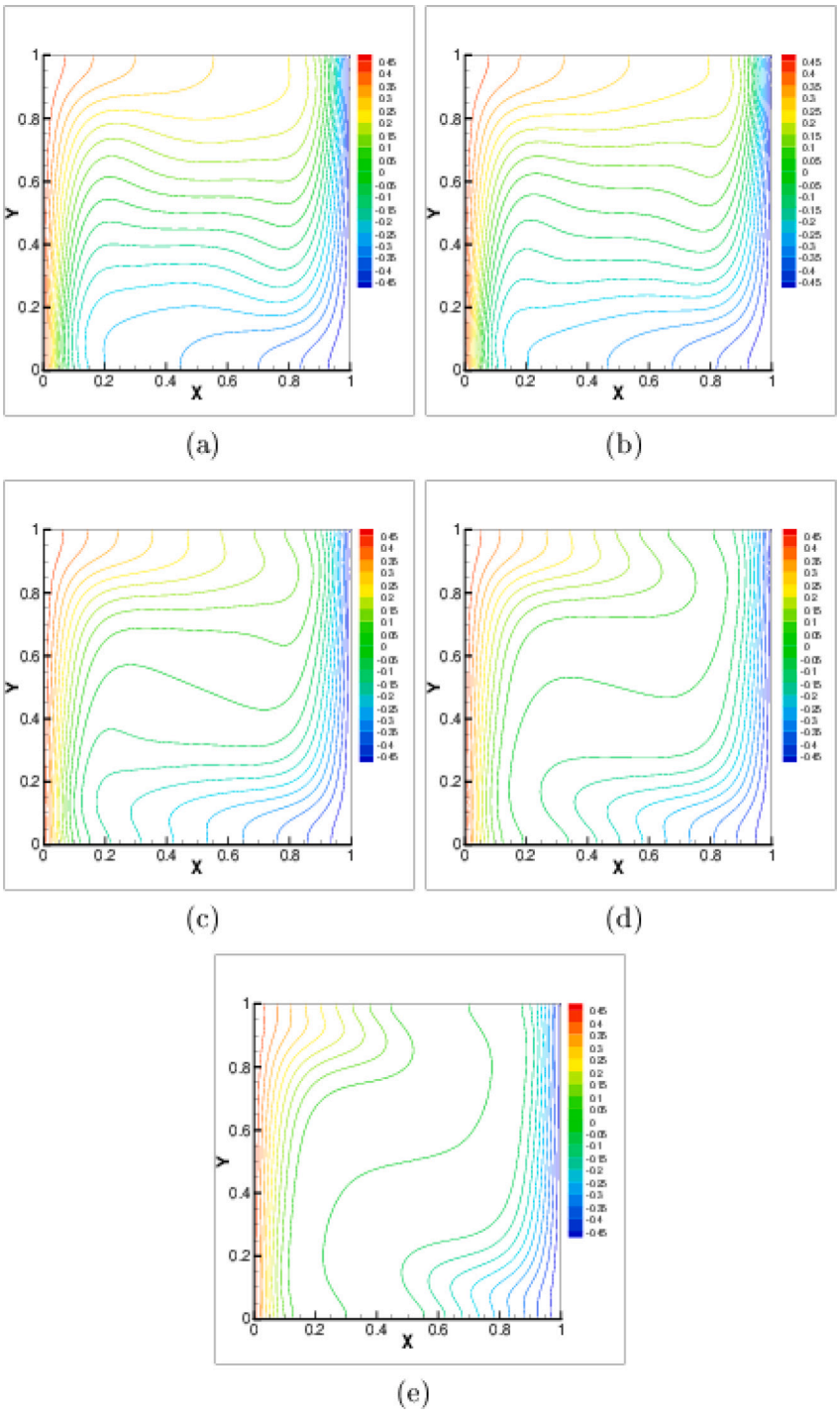

Fig. 8. Isotherms at (a) $Pr = 1$, (b) $Pr = 10$, (c) $Pr = 50$, (d) $Pr = 70$, and (e) $Pr = 100$ when $Ra = 10^5$.

goes down against Pr because heat convection loses its domination gradually. Since $Pr > 70$, heat conduction plays a critical role and few of isotherms are horizontal (refer to Fig. 8(e)). Consequently, Nu grows up monotonically with Pr again within this range.

For the situations with $Ra = 10^6$, the driving force due to heat convection is the strongest in the all cases investigated in this work. Consequently, the contribution of heat conduction becomes the weakest. As plotted by Fig. 9(d), even for $Pr = 100$, there are many horizontal isotherms in the center of the cavity, which represents the contribution due to heat convection is still comparable to that due to heat conduction. Within this competitive range, it is sure that Nu will descend against Pr, consistent with the above

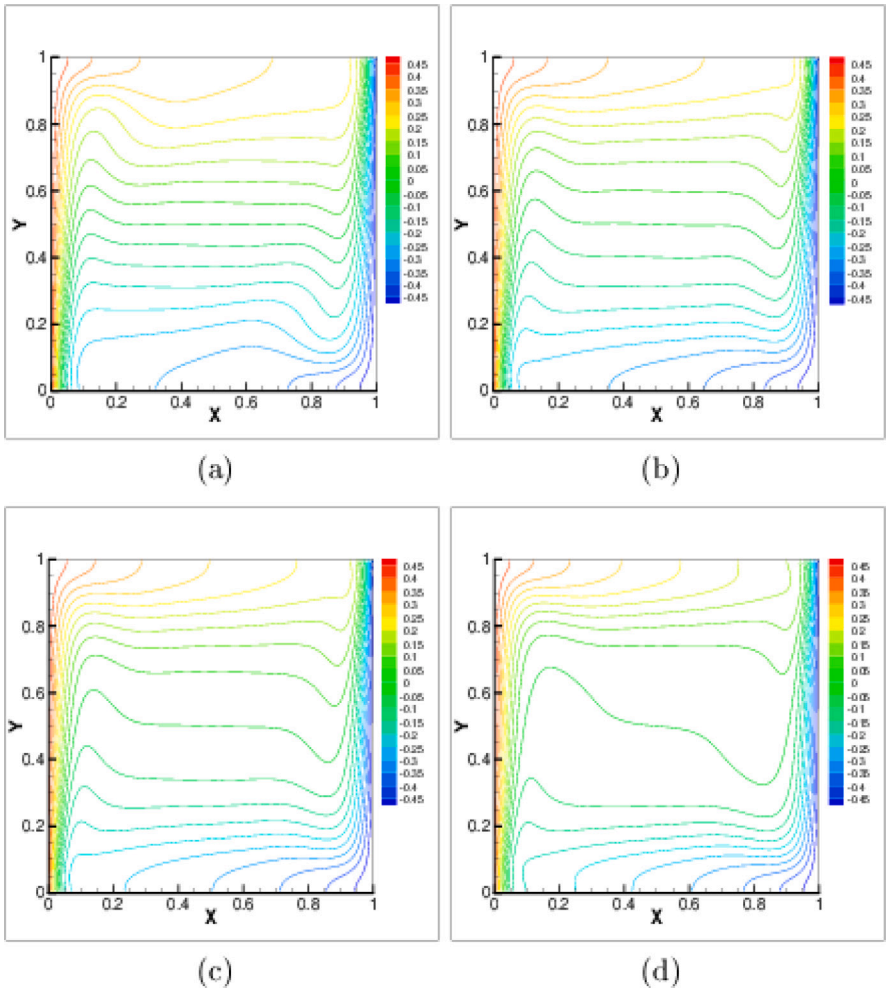

Fig. 9. Isotherms at (a) $Pr = 1$, (b) $Pr = 10$, (c) $Pr = 30$ and (d) $Pr = 100$ when $Ra = 10^6$.

observation. While $Pr < 10$, compared to heat convection, the contribution of heat conduction can be neglected, so Nu is augmented by Pr, which also agrees with the above analysis.

Based on the above analyses, it may conclude there exist two critical Prandtl numbers, i.e. Pr_1 and Pr_2 illustrated in Fig. 5, to describe the correlation between Nu and Pr. If $Pr < Pr_1$, natural convection is dominated by heat convection and Nu will ascend with Pr. While $Pr_1 < Pr < Pr_2$ where the contribution due to heat convection and that due to heat conduction are comparable, Nu will go down against Pr. For $Pr > Pr_2$, heat conduction overweighs heat convection completely, and Nu will climb up again with Pr. In this work, these characteristic ranges are defined as: the heat-convection-dominated range ($Pr < Pr_1$), the transition range ($Pr_1 < Pr < Pr_2$), and the heat-conduction-dominated range ($Pr > Pr_2$). In each characteristic range, the correlation between Nu and Pr is monotonic. For the present investigated cases, Pr_1 is nearly insensitive to Ra and in the vicinity of 10. However, Pr_2 depends significantly on Ra critically and increases obviously with Ra. If natural convection is very weak (e.g. $Ra = 10^3$), Pr_1 may not appear. And vice verse, if natural convection is always strong enough (e.g. $Ra = 10^6$), it is too difficult to observe the emergence of Pr_2.

Consequently, when extracting a correlation between Nu and Pr for natural convection, firstly the researchers should identify to which characteristic range their investigation belongs, namely identifying Pr_1 and Pr_2 for their investigated cases. The correlations extracted from different characteristic ranges are completely opposing, which can answer the conflict raised by previous publications.

6. Conclusion

In this work, to extend the LBM to simulate natural convection of large Pr working fluids, an MRT thermal LB model is developed and used to investigate numerically the natural convection in a square cavity. Through analyzing the numerical results, for the first time, it is found that there are three characteristic ranges of natural convection, divided by two critical Prandtl numbers (Pr_1 and

Pr_2). In each range, the predominant heat transfer mechanism is different, which will cause completely opposing trends of variation between Nu and Pr. In the heat-conduction-dominated range and heat-convection-dominated range, Nu will increase monotonically with Pr. However, in the so-called transition range where convection and conduction are competitive, Nu will be a monotonic decreasing function of Pr. The new findings of this work can sort out a controversy in the area of natural convection research, namely why completely opposing statements on the correlation between Nu and Pr were published in the previous literature. In future studies, when discussing the correlation between Nu and Pr, first of all, researchers should identify whether their investigated cases fall into different characteristic ranges of natural convection.

Nomenclature

Nu Nusselt number
Ra Rayleigh number
F external force
c_s speed of sound
Pr Prandtl number
u velocity
t time
T temperature
p pressure
g gravity
f, g distribution function
$\mathbf{M}, \mathbf{N}$ transformation matrix
$\mathbf{S}$ relaxation matrix
e_k discrete direction

subscript and superscript

eq equilibrium function
j, k space tensor

Greek symbols

ν kinematic viscosity
α thermal diffusivity
τ relaxation time
η model parameter

CRediT authorship contribution statement

Sheng Chen: Investigation, Methodology, Writing – original draft. **Kai H. Luo:** Project administration, Writing – review & editing, Funding acquisition. **Amit Kumar Jain:** Validation. **Dharminder Singh:** Formal analysis. **Don McGlinchey:** Writing – review & editing.

Declaration of competing interest

The authors declare that they have no known competing financial interests or personal relationships that could have appeared to influence the work reported in this paper.

Data availability

Data will be made available on request.

Acknowledgments

Support from the UK Engineering and Physical Sciences Research Council under the project UK Consortium on Mesoscale Engineering Sciences (UKCOMES) (Grant No. EP/R029598/1) is gratefully acknowledged.

Appendix

To derive the macroscopic heat transfer governing equation (3) from the D2Q5 MRT-LB equation (4), the following multiscale expansions in time and space are introduced [31]:

$$\mathbf{m} = \mathbf{m}^{(0)} + \epsilon\mathbf{m}^{(1)} + \epsilon^2\mathbf{m}^{(2)} + \cdots \tag{20}$$

$$\partial_t = \epsilon\partial_{t_1} + \epsilon^2\partial_{t_2} \tag{21}$$

$$\nabla = \epsilon\nabla_1 \tag{22}$$

Then one can obtain the following equations in the order of ϵ:

$$\epsilon^0 : \mathbf{m}^{(0)} = \mathbf{m}^{(eq)} \tag{23}$$

$$\epsilon^1 : D_1\mathbf{m}^{(0)} = -\mathbf{S}\mathbf{m}^{(1)} \tag{24}$$

$$\epsilon^2 : \partial_{t_2}\mathbf{m}^{(0)} + D_1(\mathbf{I} - \frac{\mathbf{S}}{2})\mathbf{m}^{(1)} = -\mathbf{S}\mathbf{m}^{(2)} \tag{25}$$

where $D_1 = (\partial_{t_1} + \nabla_1)$ and $\mathbf{I}$ is a unit matrix. With the aid of the above equations, one can get:

$$\partial_{t_1}\frac{T}{\eta} + \nabla_{x_1}\frac{u_xT}{\eta} + \nabla_{y_1}\frac{u_yT}{\eta} = 0 \tag{26}$$

$$\partial_{t_1}\frac{u_xT}{\eta} + \nabla_{x_1}\frac{T}{5} = -\tau_\Theta^{-1}m_1^{(1)} \tag{27}$$

$$\partial_{t_1}\frac{u_yT}{\eta} + \nabla_{y_1}\frac{T}{5} = -\tau_\Theta^{-1}m_2^{(1)} \tag{28}$$

$$\partial_{t_2}\frac{T}{\eta} + \nabla_{x_1}[(1 - \frac{\tau_\Theta^{-1}}{2})m_1^{(1)}] + \nabla_{y_1}[(1 - \frac{\tau_\Theta^{-1}}{2})m_2^{(1)}] = 0 \tag{29}$$

and

$$m_1^{(1)} = -\tau_\Theta[\partial_{t_1}\frac{u_xT}{\eta} + \frac{1}{5}\nabla_{x_1}T] \tag{30}$$

$$m_2^{(1)} = -\tau_\Theta[\partial_{t_1}\frac{u_yT}{\eta} + \frac{1}{5}\nabla_{y_1}T] \tag{31}$$

With the aid of Eqs. (26)–(31), one can obtain

$$\partial_t\frac{T}{\eta} + \nabla_x\frac{u_xT}{\eta} + \nabla_y\frac{u_yT}{\eta} = \frac{\Delta t}{5}(\tau_\Theta - 0.5)(\nabla_x^2T + \nabla_y^2T) \tag{32}$$

From Eq. (32), one can get

$$\partial_tT + \nabla_x(u_xT) + \nabla_y(u_yT) = \frac{\eta}{5}(\tau_\Theta - 0.5)\Delta t(\nabla_x^2T + \nabla_y^2T) \tag{33}$$

If one define $\alpha = \frac{\eta}{5}(\tau_\Theta - 0.5)\Delta t$, Eq. (33) is the same as the governing equation (3).

References

[1] M.H. Abdel-AzizG, H. Sedahmed, Natural convection mass and heat transfer at a horizontal spiral tube heat exchanger, Chem. Eng. Res. Des. 145 (2019) 122–127.

[2] A.J. Chamkha, Double-diffusive convection in a porous enclosure with cooperating temperature and concentration gradients and heat generation or absorption effects, Numer. Heat Transfer Part A Appl. 41 (2002) 65–87.

[3] S. Izadi, T. Armaghani, R. Ghasemiasl, A.J. Chamkha, M. Molana, A comprehensive review on mixed convection of nanofluids in various shapes of enclosures, Powder Technol. 343 (2019) 880–907.

[4] A.S. Dogonchi, A.J. Chamkha, D.D. Ganji, A numerical investigation of magneto-hydrodynamic natural convection of Cu–water nanofluid in a wavy cavity using CVFEM, J. Therm. Anal. Calorim. 135 (2019) 2599–2611.

[5] I.V. Shevchuk, A new evaluation method for nusselt numbers in naphthalene sublimation experiments in rotating-disk systems, Heat Mass Transf. 44 (2008) 1409–1415.

[6] I.V. Shevchuk, An integral method for turbulent heat and mass transfer over a rotating disk for the Prandtl and Schmidt numbers much larger than unity, Heat Mass Transf. 45 (2009) 1313–1321.

[7] I.V. Shevchuk, Modelling of convective heat and mass transfer in rotating flows, in: Mathematical Engineering, Springer, 2016.

[8] S. Pandey, Y. Park, M. Ha, An exhaustive review of studies on natural convection in enclosures with and without internal bodies of various shapes, Int. J. Heat Mass Transfer 138 (2019) 762–795.

[9] W. Zhou, H.I. Mohammed, S. Chen, M. Luo, Y. Wu, Effects of mechanical vibration on the heat transfer performance of shell-and-tube latent heat thermal storage units during charging process, Appl. Therm. Eng. 216 (2022) 119133.

[10] W. Du, S. Chen, Effect of mechanical vibration on phase change material based thermal management module of a lithium-ion battery at high ambient temperature, J. Energy Storage 59 (2023) 106465.
[11] Q. Li, C. Wang, C. Wang, T. Zhou, X. Zhang, Y. Zhang, W. Zhuge, L. Sun, Comparison of organic coolants for boiling cooling of proton exchange membrane fuel cell, Energy 266 (2023) 126342.
[12] M. Gourdon, E. Karlsson, F. Innings, A. Jongsma, L. Vamling, Heat transfer for falling film evaporation of industrially relevant fluids up to very high Prandtl numbers, Heat Mass Transfer 52 (2016) 379–391.
[13] S. Das, P. Bhattacharya, Effect of Prandtl number on laminar natural convective heat transfer inside cavity, Procedia Eng. 127 (2015) 229–234.
[14] S. Hsieh, C. Wang, Experimental study of three-dimensional natural convection in enclsures with different working fluids, Int. J. Heat Mass Transfer 37 (1994) 2687–2698.
[15] O. Shishkina, M. Emran, S. Grossmann, D. Lohse, Scaling relations in large-Prandtl-number natural thermal convection, Phys. Rev. Fluids 2 (2017) 103502.
[16] B. Dubrulle, Scaling in large Prandtl number turbulent thermal convection, Eur. Phys. J. B 28 (2002) 361–367.
[17] Q. Al-Amir, S. Ahmed, H. Hamzah, F. Ali, Effects of Prandtl number on natural convection in a cavity filled with silver water nanofluid-saturated porous medium and non-Newtonian fluid layers separated by sinusoidal vertical interface, Arab. J. Sci. Eng. 44 (2019) 10339–10354.
[18] T. Basak, S. Roy, A. Balakrishnan, Effects of thermal boundary conditions on natural convection flows within a square cavity, Int. J. Heat Mass Transfer 49 (2006) 4525–4535.
[19] A. D'Orazio, A. Karimipour, A useful case study to develop lattice Boltzmann method performance: Gravity effects on slip velocity and temperature profiles of an air flow inside a microchannel under a constant heat flux boundary condition, Int. J. Heat Mass Transfer 136 (2019) 1017–1029.
[20] M. Goodarzi, A. Drazio, A. Keshavarzi, S. Mousavi, A. Karimipour, Develop the nano scale method of lattice Boltzmann to predict the fluid flow and heat transfer of air in the inclined lid driven cavity with a large heat source inside two case studies: pure natural convection and mixed convection, Physica A 509 (2018) 210–233.
[21] H. Sajjadi, A. Delouei, M. Atashafrooz, M. Sheikholeslami, Double MRT lattice Boltzmann simulation of 3-D MHD natural convection in a cubic cavity with sinusoidal temperature distribution utilizing nanofluid, Int. J. Heat Mass Transfer 126 (2018) 489–503.
[22] Y. Cao, Y. Zhang, Investigation on the natural convection in horizontal concentric annulus using the variable property-based lattice Boltzmann flux solver, Int. J. Heat Mass Transfer 111 (2017) 1260–1271.
[23] Y. Feng, S. Guo, W. Tao, P. Sagaut, Regularized thermal lattice Boltzmann method for natural convection with large temperature differences, Int. J. Heat Mass Transfer 125 (2018) 1379–1391.
[24] S. Polasanapalli, K. Anupindi, A high-order compact finite-difference lattice Boltzmann method for simulation of natural convection, Comput. Fluids 181 (2019) 259–282.
[25] K. Sharma, R. Straka, F. Tavares, Natural convection heat transfer modeling by the cascaded thermal lattice Boltzmann method, Int. J. Therm. Sci. 134 (2018) 552–564.
[26] X. Feng, Q. Liu, Y. He, Numerical simulations of convection heat transfer in porous media using a cascaded lattice Boltzmann method, Int. J. Heat Mass Transfer 151 (2020) 119410.
[27] D. Dapelo, S. Simonis, M.J. Krause, J. Bridgeman, Lattice-Boltzmann coupled models for advection-diffusion flow on a wide range of pḷet numbers, J. Comput. Sci. 51 (2021) 101363.
[28] S. Chen, B. Yang, K.H. Luo, X. Xiong, C. Zheng, Double diffusion natural convection in a square cavity filled with nanofluid, Int. J. Heat Mass Transfer 95 (2016) 1070–1083.
[29] S. Chen, M. Krafczyk, Entropy generation in turbulent natural convection due to internal heat generation, Int. J. Therm. Sci. 48 (2009) 1978–1987.
[30] S. Chen, B. Yang, C. Zheng, Simulation of double diffusive convection in fluid-saturated porous media by lattice Boltzmann method, Int. J. Heat Mass Transfer 108 (2017) 1501–1510.
[31] M. Jami, F. Moufekkir, A. Mezrhab, J. Fontaine, M. Bouzidi, New thermal MRT lattice Boltzmann method for simulations of convective flows, Int. J. Therm. Sci. 100 (2016) 98–107.
[32] S. Chen, H. Liu, C. Zheng, Numerical study of turbulent double-diffusive natural convection in a square cavity by LES-based lattice Boltzmann model, Int. J. Heat Mass Transfer 55 (2012) 4862–4870.